Transition State of the Rate-Limiting Step of Heat Denaturation of Cry3A δ-Endotoxin†

Sergey A. Potekhin,*,‡ Olga I. Loseva,§ Elizabeth I. Tiktopulo,‡ and Anatoly P. Dobritsa§

Institute of Protein Research, Russian Academy of Sciences, 142292 Pushchino, Moscow Region, Russia, and State Research Center for Applied Microbiology, 142279 Obolensk, Moscow Region, Russia

Received November 24, 1998; Revised Manuscript Received January 27, 1999

ABSTRACT: Heat denaturation of Cry3A δ-endotoxin from *Bacillus thuringiensis* var. *tenebrionis* and its 55 kDa fragment was studied by differential scanning microcalorimetry at low pH. Analysis of the calorimetric data has shown that denaturation of Cry3A δ-endotoxin is a nonequilibrium process at heating rates from 0.125 to 2 K/min. This means that the stability of δ-endotoxin (the apparent temperature of denaturation T_m) under these conditions is under kinetic control rather than under thermodynamic control. It has been shown that heat denaturation of this protein is a one-step kinetic process. The enthalpy of the process and its activation energy were measured as functions of temperature. The data obtained allow confirmation of the fact that the conformation of δ-endotoxin at the transition state only slightly differs from its native conformation with respect to compactness and extent of hydration. The comparison of the activation energy for intact δ-endotoxin and the 55 kDa fragment showed that the transition of the molecule to a transition state does not cause any changes in the conformation of three N-terminal α-helices. Complete removal of the N-terminal domain of δ-endotoxin and 40 amino acids from the C-terminus β-sheet domain III causes an irreversible loss of the tertiary structure. Thus, during protein folding the nucleation core determining protein stability does not involve its three initial α-helices but may include the remaining α-helices of the N-terminal domain. The functional significance of peculiarities of structure arrangement of the δ-endotoxin molecule is discussed.

It is known that the rate of protein folding and/or unfolding is determined by the free energy of the transition state relative to that of the initial state. By definition, the transition state is most unfavorable energetically. This state is virtual. The lifetime and population of this state are very low under any conditions. Thus, it is practically impossible to study structural peculiarities of this state in equilibrium or kinetic experiments. But it is tempting to obtain such information for several reasons. Most important is the fact that the structure of the transition state and the energetic barrier between the folding and unfolding states is the key for understanding the origin of the cooperativity of the molecule.

Thus, the only way to obtain any information about the transition state is to keep track of constant rate and activation energy dependence on conditions and protein structure. Then we can use our knowledge about the correlation between structural and energetic parameters to clarify some structural features of the transition state.

Bacillus thuringiensis is a Gram-positive bacterium that forms paraspore crystalline protein inclusions (δ-endotoxins) during sporulation which can be toxic to insects and some other organisms. δ-Endotoxins are present in crystals as inactive protoxins. In insect midgut, the crystals are dissolved, and protoxins are processed by gut proteases and turn into active toxins (*1*−*3*). The *cry*3A gene specifies the synthesis of the 72 kDa protoxin in *Bacillus thuringiensis* var. *tenebrionis*. When 57 amino acids are removed from the N-terminus by endogenous proteases, an active toxin with a molecular mass of 67 kDa is formed (*4*, *5*).

δ-Endotoxins from *B. thuringiensis* (Bt) form pores in the midgut epithelium of susceptible insects. This leads to a disturbance in the osmotic balance, lysis of cells, and, finally, death of insects (*3*, *6*). It is suggested that during receptor binding and pore formation δ-endotoxin molecules undergo large-scale conformational changes whose character remains yet unclear. Such changes should be studied to clarify the mechanism of pore formation and to enable production of more efficient biopesticides. All available models of pore formation are hypothetical and should be studied further (*7*, *8*).

It is clear that significant alterations in the relative positioning of different parts of the molecule can occur only if the structural regions do not form a cooperative system. Scanning microcalorimetry provides a most direct approach for revealing cooperative regions within protein molecules (*9*−*12*). However, the thermodynamic analysis of calorimetric curves requires the denaturation process to proceed under equilibrium conditions which does not always take place. In many cases, heat denaturation of proteins is a kinetically driven process. In such cases, the shape of melting curves can provide very useful information about kinetic parameters of denaturation (*13*−*16*).

† This work was supported in part by the International Science and Technical Center (Grant 363).

* Corresponding author. Phone or fax: (7-095)924-0493. E-mail: spot@sun.ipr.serpukhov.su.

‡ Russian Academy of Sciences.

§ State Research Center for Applied Microbiology.

10.1021/bi982789k CCC: $18.00
Published on Web 03/11/1999

We have shown previously (*17*) that the heat denaturation of Cry3A δ-endotoxin under alkaline conditions (pH 9.7−11.0) is consistent with the van't Hoff model; i.e., the protein melts at equilibrium as a single cooperative domain. In contrast, calorimetric curves obtained at pH 2.2−3.5 do not correspond to this model. Such a discrepancy can be caused both by the complex (multidomain) structure of the molecule and by the metastability of its structure. The results of this study elucidate the nature of the stability of the δ-endotoxin structure at low pH and demonstrate some structural properties of the transition state for this molecule.

MATERIALS AND METHODS

The cells of *B. thuringiensis* var. *tenebrionis* were cultivated on the Ches medium (*18*) as described in ref *19*. Proteolysis of the 72 kDa protoxin to the 67 kDa toxin was the result of associated endogenous proteinase activity after crystal release. The suspension of spores and crystals was fractionated by using gradients of 67, 72, and 82% (w/v) sucrose in distilled water (*20*). The 55 kDa fragment of Cry3A δ-endotoxin was obtained by trypsin (Spofa) proteolysis (*20*). The 37 kDa fragment was obtained by pepsin (Sigma) proteolysis (*21*). The purified crystals and obtained fragments were dissolved in 100 mM glycine hydrochloride buffer (glycine-HCl) at pH 3.0 at 37 °C for 1 h. The insoluble material was separated by centrifugation, and the supernatant was dialyzed against 25 mM glycine-HCl at pH 2.0−3.5 overnight at 4 °C.

The homogeneity of the protein preparations was analyzed by polyacrylamide gel electrophoresis (*22*). A PAGE linear gradient (10 to 15%) was used as a separating gel. The protein concentration was determined according to the methods of Lowry et al. (*23*) with bovine serum albumin (Sigma) as a standard.

The circular dichroism spectra (CD)[1] were measured using a JASCO-41A spectropolarimeter. The molar ellipticity was calculated from the equation $[\theta] = \theta_{obs}M_{res}/(cl)$, where c is the protein concentration (grams per milliliter), l is the optical path length of the cell (millimeters), θ_{obs} is the ellipticity measured (degrees) at wavelength λ, and M_{res} is the mean residue molecular mass estimated from the amino acid content of the proteins.

Calorimetric measurements were taken on a DASM-4A precision scanning microcalorimeter ("Biopribor", Pushchino, Russia) with golden cells with a volume of 0.5 mL and on a SCAL-1 scanning microcalorimeter (Scal Co. Ltd., Pushchino, Russia) with glass cells with a volume of 0.3 mL at scanning rates from 0.125 to 2.0 K/min. Despite noticeable differences in the dynamic characteristics of the instruments, the obtained kinetic and thermodynamic parameters did not vary appreciably. The assessment of the protein relaxation time (*26*) at the apparent temperature of transition and the heating rate of 1 K/min showed that under experimental conditions this value ranges from 130 to 180 s, which is much higher than the response time of the instruments used.

Degassing during the calorimetric experiments was prevented by maintaining an additional constant pressure of 2.5 atm over the liquids in the cells. The experiments were performed in 25 mM glycine-HCl solution at pH 2.0−3.5. The reversibility of transitions was checked by reheating the solution in the calorimetric cell after cooling from the first run. In all cases, the thermal denaturation of δ-endotoxin and the 55 kDa fragment was found to be irreversible. The protein concentration in the experiments varied from 0.4 to 4.5 mg/mL. No concentration dependence of the kinetic and thermodynamic parameters was detected with a more than 10-fold change in the protein concentration. The experimental calorimetric traces were corrected for the calorimetric baseline, and the molar partial heat capacity functions were calculated in a standard manner. The excess heat capacity was evaluated by subtraction of the linearly extrapolated initial and final heat capacity functions with correction for the difference of these functions by using a sigmoidal baseline (*11*). A typical value for the partial specific volume for globular proteins (0.73 cm^3/g) was accepted arbitrarily, since it does not influence the calculated excess heat capacity.

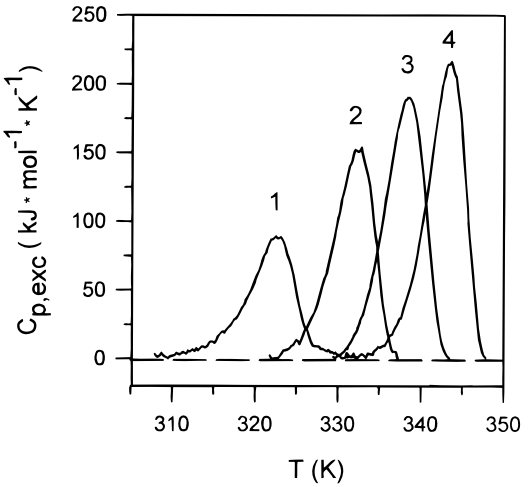

FIGURE 1: Dependence of the excess partial heat capacity of δ-endotoxin on temperature at different pHs. Curves 1−4 correspond to pH 2.0, 2.5, 3.0, and 3.5, respectively. The curves were obtained at a heating rate of 1 K/min.

RESULTS

Figure 1 shows the temperature dependence of the partial molar heat capacity for toxin Cry3A at pH 2.0−3.5. Thermodynamic parameters of denaturation are listed in Table 1.

A specific feature of the obtained curves is asymmetry of the excess heat absorption peaks. There may be two reasons for this: (1) the denaturation being a multistage process and/or (2) kinetic character of the observed transition. The latter is reasonable since repeated heating of the samples revealed almost complete irreproducibility of denaturation curves upon recurrent heating. However, the irreproducibility established in such a way is not always pure thermodynamic irreversibility (*11*, *24*) and may be caused by slow processes following equilibrium denaturation, e.g. slow chemical modifications or aggregation. In such cases, the shape of melting curves is not practically distorted and can be treated using equilibrium thermodynamics. The possible reason for the irreproducibility of Cry3A δ-endotoxin is the protein propensity to aggregate in a denatured state. Though the heated protein solution remains pellucid at temperatures higher than the denaturation temperature, it becomes turbid

[1] Abbreviations: DSC, differential scanning calorimetry; CD, circular dichroism; GdmCl, guanidinium chloride; SDS, sodium dodecyl sulfate.

Table 1: Thermodynamic and Kinetic Characteristics of Denaturation for δ-Endotoxin and Its Fragment[a]

	pH	T_m (K)	ΔH_m (kJ/mol)	ΔE_{uf} (kJ/mol)	V (K/min)	α
δ-endotoxin	3.5	343.6	1330	464	1.00	1.77
	3.0	340.4	1300	393	2.00	1.65
		338.6	1200	410	1.00	1.62
		337.0	1210	389	0.50	1.74
		333.5	945	405	0.125	1.87
	2.8	333.1	849	389	1.00	1.54
		331.7	840	380	0.125	1.81
	2.5	332.5	924	405	1.00	1.80
	2.0	322.7	644	330	1.00	1.62
55 kDa fragment	3.0	343.3	832	468	1.00	1.89
	2.75	334.3	815	364	1.00	1.74
	2.5	330.7	727	385	1.00	1.65
	2.0	322.2	652	288	1.00	1.60

[a] T_m is the temperature of the peak maximum. ΔH_m is the calorimetric enthalpy. ΔE_{uf} is the activation energy. V is the scanning rate. α is the extent of asymmetry of peaks (the ratio of the heat revealed below ΔQ_- and above ΔQ_+ T_m).

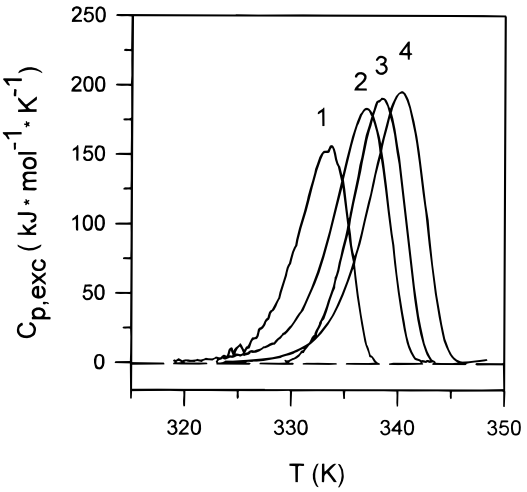

FIGURE 2: Dependence of the excess partial heat capacity of δ-endotoxin on temperature at pH 3.0 and different heating rates: (1) 0.125, (2) 0.5, (3) 1.0, and (4) 2.0 K/min, respectively.

after cooling. Therefore, before using any model for analysis, denaturation and respective calorimetric profiles should be studied in detail.

To verify whether the denaturation process is equilibrium, melting curves have been obtained at different heating rates. Figure 2 shows that they have a noticeable shift in temperature depending on the heating rate which is evidence of nonequilibrium conditions of the experiment. This means that denaturation under the given conditions is thermodynamically irreversible or the heating rates are too high to consider this process an equilibrium. It has been shown previously (*14*, *25*, *26*) that both cases will lead to similar shapes for the melting curve. Indeed, even when protein denaturation is reversible and proceeds in one stage, the heating rates significantly exceed the value

$$V_{max} = \frac{RT_d^2}{\Delta H_m \tau_d} \quad (1)$$

where T_d is the real (equilibrium) temperature of denaturation, ΔH_m is the enthalpy, τ_d is the relaxation time, and R is the universal gas constant, and the melting curves would be described well by the irreversible kinetic scheme

$$N \xrightarrow{k} D \quad (2)$$

The other problem that should be clarified is the number of stages in the given kinetic process (the number of states realized upon increasing the temperature). It was demonstrated (*25*) that the extent of asymmetry α of peaks (the ratio of the heat revealed below ΔQ_- and above ΔQ_+ the transition temperature T_m) for irreversible (and consequently nonequilibrium) one-stage processes is bound to be

$$\alpha = \frac{\Delta Q_-}{\Delta Q_+} = e - 1 \approx 1.72 \quad (3)$$

A calculation of this coefficient for experimental curves shows (Table 1) that the experimental curves are in good agreement with the kinetic model of transition between the two states as determined by these criteria.

The conclusion that the process has one stage is also corroborated by the fact that preliminary heating of the protein solution to the transition region causes a decrease in the heat absorption peak area, but does not change its shape. The curve can be obtained from the initial curve just by normalizing it. This is not expected for the multistage process, for which distortion of the curve should occur because of a different characteristic temperature and a constant rate and extent of reversibility for different stages. As a result, their relative contribution to the net calorimetric curve should change.

A more direct way to check the correspondence of the denaturation transition to such a model is to find a possibility of describing experimental curves with model ones. It is known (*14*, *15*, *27*) that a shape of the heat absorption curve for an irreversible one-stage process is described by

$$c_{p,exc} = e c_p^{max} \exp\left[\frac{\Delta E_{uf}(T - T_m)}{RT_m^2}\right] \times \exp\left\{\exp\left[\frac{\Delta E_{uf}(T - T_m)}{RT_m^2}\right]\right\} \quad (4)$$

where T_m is the apparent temperature of denaturation and ΔE_{uf} is the activation energy.

The function depends on three parameters: T_m, c_p^{max}, and ΔE_{uf}. In general, these parameters are not independent and are coupled by the ratio (*13*, *28*)

$$\Delta E_{uf} = \frac{eRT_m^2 c_p^{max}}{\Delta E_m} \quad (5)$$

Using the least-squares method, we determined the parameters corresponding to the best description of experimental curves. Initial values for the activation energy were evaluated with eq 5. Figure 3 shows examples for such a description. As seen from the figure, excess heat absorption curves are compatible with the kinetic one-stage model. The kinetic parameters of transitions are listed in Table 1.

One more circumstance should be taken into account. Activation energy values can be estimated in two ways: either from the shape of the curves as was demonstrated previously or from the dependence of the apparent denatur-

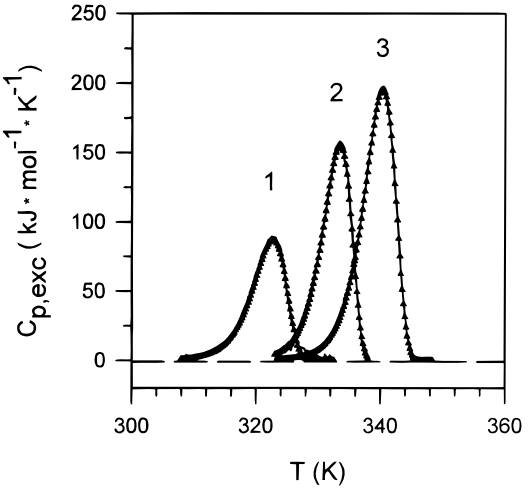

FIGURE 3: Best fit (▲) of the experimental excess heat capacity functions of δ-endotoxin (solid lines) using a one-stage kinetic model: (1) pH 2.0, $V = 1.0$ K/min; (2) pH 3.0, $V = 0.125$ K/min; and (3) pH 3.0, $V = 2$ K/min.

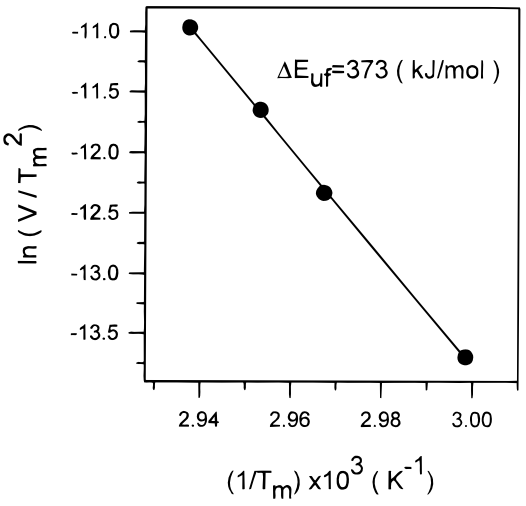

FIGURE 4: Dependence of $\ln(V/T_m^2)$ on the apparent denaturation temperature T_m. Experimental points were obtained at pH 3.0 and heating rates (V) of 2.0, 1.0, 0.5, and 0.125 K/min.

ation temperature T_m on the heating rate (*14*). Figure 4 gives this dependence. The function is linear which suggests nonequilibrium melting even at the minimal heating rate studied. The activation energy values calculated from this dependence and directly from the shape of the curves (Table 1 and Figure 5) are compatible. This fact additionally corroborates the correspondence of the experimental data to the model used.

Figure 5 shows the dependence of the activation energy of denaturation. On the basis of transition-state theory, the activation energy is approximately equal to the enthalpy of this state. The function is linear and increases slightly with a temperature increase. The dependence of the denaturation enthalpy is also given there. It is known that the denaturation enthalpy of proteins is practically independent of solution pH (*29*) and is a function of temperature only. Abnormal titration of groups that can occur upon denaturation does not contribute noticeably to the denaturation enthalpy at least at low pH. The same assumption may be also taken for the activation energy (*30*−*32*). This means that the slope of the dependencies given in Figure 5 should coincide with the corresponding heat capacity increments. Their values are 33.0

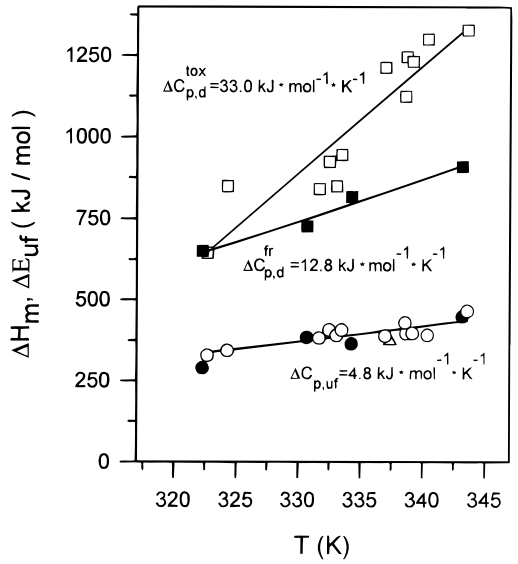

FIGURE 5: Dependence of enthalpy (squares) and activation energy (circles) of denaturation on the apparent denaturation temperature T_m. The activation energy obtained from experiments on the dependence of the apparent melting temperature on the heating rate (Figure 4) is depicted with a white triangle. The data for the intact molecule are depicted with white symbols, while those for the 55 kDa fragment are depicted with black symbols. Straight lines are drawn by the least-squares method and correspond to heat capacity increments given in the figure.

and 4.8 kJ mol^{-1} K^{-1} for denaturation and activation, respectively; i.e., during transition to the activated state, the change of the toxin heat capacity does not exceed 15% of the heat capacity increment for denaturation.

In addition to the 67 kDa Cry3A toxin, its two fragments, 55 and 37 kDa, were also studied. At present, the three-dimensional structures of the Cry3A and Cry1Aa toxins have been solved (*33*, *34*). The toxins have similar conformations; they are wedge-shaped molecules and consist of three structural domains: one α-helical domain (I) formed by a bundle of seven helical segments and domains II and III containing mostly β-sheets. The 55 kDa fragment consists of four α-helical fragments ($\alpha_4-\alpha_7$) of domain I and two β-sheet domains (*35*). The 37 kDa fragment has no α-helical domain I. It is formed of β-sheet domain II and a greater part of β-sheet domain III (*21*).

It should be noted that the 55 kDa fragment is prepared from δ-endotoxin whose crystals are preliminarily dissolved in 3.3 M KBr solution. There are no absorption peaks on the DSC traces for both preparations under this condition. The toxin molecule and its fragment reversibly lose its compact tertiary structure. After removal of KBr, molecules restore their unique tertiary structure. Thus, despite the apparent irreversibility of heat denaturation, at a low temperature both the structure of the intact protein and its 55 kDa fragment are favorable energetically. The irreversibility of heat denaturation is evidently caused by the unfavorable relation of thermodynamic and kinetic parameters and/or aggregation effects. Figure 6 shows melting curves of the 55 kDa fragment and an intact toxin molecule at pH 3.0. As seen from Figure 6 and Table 1, removal of three α-helices causes an increase in the molecule apparent stability and a significant drop of the denaturation enthalpy at this pH. However, the shape of the melting curve does not change. The melting curve of the intact protein can be obtained by

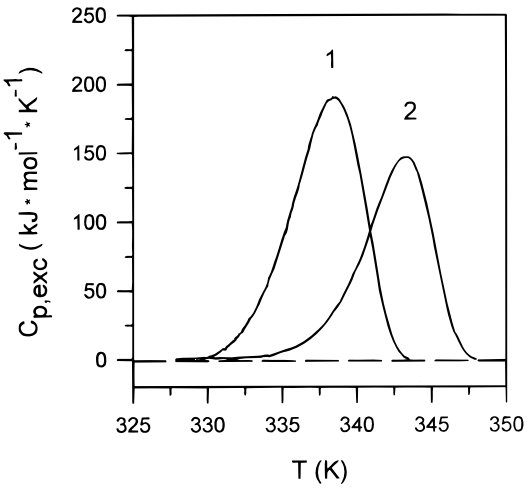

FIGURE 6: Temperature dependence of the excess heat capacity functions for δ-endotoxin (1) and its 55 kDa fragment (2) at pH 3.0 and a heating rate of 1 K/min.

normalization of the excess heat capacity of the 55 kDa fragment. Like in the case of intact protein, the curve is described well by a kinetic one-stage model. The activation energy calculated from the curve shape coincides with this function for the whole molecule (Figure 5). Thus, the energy contributions of the lacking region to the native conformation and the transition state are identical which suggests its passive role in maintaining the native structure.

The 37 kDa fragment of δ-endotoxin can be obtained only in the presence of 3.6 M guanidinium chloride (GdmCl) (*21*). Under these conditions, a molecule of the toxin loses its compact tertiary structure which is demonstrated by the absence of a heat absorption peak on DSC traces. However, like in the case with a 3.3 M KBr solution, denaturation of δ-endotoxin proved to be reversible under these conditions. In contrast, our attempts to renature the 37 kDa fragment failed. Removal of guanidine chloride caused aggregation of the obtained C-terminal fragment. We tried to restore the initial conformation of the fragment in different ways. The 37 kDa fragment which is not dissolved under standard conditions appeared to be dissolved in 0.1% SDS. But removal of SDS by acetone or prolonged dialysis did not restore the tertiary structure of the fragment causing irreversible aggregation. As shown by the CD data, a small portion of the preparation remaining in the solution after centrifugation has no ordered secondary structure. This was corroborated by the scanning microcalorimetry data. Thus, it seems that the 37 kDa fragment is not able to maintain its native conformation.

DISCUSSION

It is known that the origin of the thermal stability of proteins can be different. When it is thermodynamic stability, the ratio of populations of the native N and denatured D states is determined by the equilibrium constant K (=[D]/[N]) and does not depend on time. In its turn, the equilibrium constant is determined by the free energy of structure stabilization, i.e., by the difference of the free energy values for the denatured and native states. Therefore, the melting curves are in equilibrium and are described by the van't Hoff model (*11*, *29*) or the model of multistage denaturation (*9*−*12*).

Second, the protein structure can be metastable. The protein can remain native even at rather high temperatures when this state is not favorable from the thermodynamic point of view. Such behavior is explained by a very slow rate of denaturation at the temperature region where the Gibbs energy of structure stabilization becomes positive. Denaturation may last for many hours and even days under this condition (*27*, *32*, *36*, *37*). Corresponding DSC transitions must be analyzed on the basis of kinetic terms (*13*−*15*, *25*). The thermodynamic properties of the transition state for unfolding can be monitored directly by the unfolding rate constant since this corresponds to the free energy difference between the native protein and the transition state, i.e., the high-energy barrier that constitutes the rate-limiting step for unfolding.

In the case of Cry3A δ-endotoxin and its 55 kDa fragment, the denaturation process is compatible with the irreversible one-stage model. Consequently, heat denaturation is nonequilibrium, and proteins have no intermediate states at experimental heating rates. Nevertheless, this does not mean that the denaturation is necessarily irreversible and the native state of the protein is not favorable energetically through the temperature range. The reason may be a slow rate of denaturation at the real transition temperature T_d (*14*, *25*, *26*). In any case, an important result of this work is that the structure of δ-endotoxin in the native state is maintained because of a high activation barrier rather than because of the thermodynamic expedience of this state, at least at high temperatures. However, the native state may be favorable energetically at sufficiently low temperatures since the protein structure is restored completely after removal of GdmCl or KBr.

When the fact that denaturation of the toxin and its fragment has a nonequilibrium character is taken into account, it is possible to determine only two thermodynamic parameters for this process. They are the heat capacity increment and the denaturation enthalpy (Figure 5). For the given protein, these parameters are within a standard range of values for globular proteins (*29*). This fact and the presence of a heat absorption peak for the 55 kDa fragment suggest that the toxin fragment retains its unique tertiary structure after removal of three N-terminal α-helices.

An interesting peculiarity of the toxin structure is that removal of three initial N-terminal α-helices leads to stabilization of the remaining part by approximately 5−6 °C at pH 3.0 (Figure 6). This is caused by a decrease of the denaturation rate for the 55 kDa fragment as compared to that of the intact molecule at the same temperature. A reason for slowing can be only a predominant decrease of the entropy of the molecule in the transition state as compared to that in the native one. However, the stabilization is pH-dependent, and at pH 2.0, the stability of the fragment is already smaller than that of the intact molecule (Table 1). Thus, the entropy contribution stabilizing the fragment with respect to the intact molecule may be dependent on the electrostatic interactions, at least partially.

Figure 5 shows that ΔE_{uf} is positive up to very low temperatures. Hence, the rate of denaturation should increase when the temperature increases, because the derivative of the rate constant for any process with respect to the temperature is proportional to the activation energy of the process. The ratio of the denaturation enthalpy to the

activation energy depends strongly on temperature. Taking into account the fact that for one-step denaturation the enthalpy should be connected with the activation energies for direct and reverse processes

$$\Delta H_m = \Delta E_{uf} - \Delta E_f \quad (6)$$

we can readily calculate the activation energy of renaturation. It is clear that this value changes its sign in the temperature range of 300−310 K. Consequently, the rate of renaturation must reach its maximal value in this temperature range and decrease with both decreasing and increasing temperatures. Such a behavior of denaturation and/or renaturation rates is common for proteins (*30*, *38*, *39*).

Several conclusions can be drawn about the structure of the transition state for δ-endotoxin. As seen from Figure 5, the heat capacity increment for the transition state is significantly smaller than the heat capacity increment for denaturation, much as was demonstrated previously for lysozyme (*30*). Since the heat capacity increment correlates well with the hydrophobic surface exposure during the conformational transition (*29*), it should be accepted that the transition state of δ-endotoxin is only slightly distinct from the native state in the exposure of hydrophobic groups and, hence, is as compact as the native one. So, we have to accept the fact that the energy barrier between native and denatured conformations exists due to the necessity of disruption of short-range interactions in certain parts of the molecule. Additionally, a large value of the activation energy strongly suggests that this disruption has a collective origin. It is consistent also with results demonstrated previously for barnase (*40*) and cold-shock protein CspB (*38*), but not for chymotrypsin inhibitor 2. In the last case, the increment of heat capacity for the transition state is intermediate between the native and denatured conformations (*41*). In agreement with experimental observations, theoretical studies suggest that the transition state is an expanded form of the native state in which a significant part of the van der Waals energy is lost, but the degree of expansion is insufficient to permit rotational isomers of the side chains or penetration of water (*42*).

The data obtained allow us to localize the nucleation core that maintains the unique structure of δ-endotoxin and in which conformational changes take place at the transition state. It is very important that removal of three N-terminal α-helices does not change the activation energy. This means that the energy contributions of these helices to the enthalpy of native and transition states are identical. In other words, this region does not undergo any conformational changes at the transition state. In contrast to the 55 kDa fragment, the 37 kDa fragment involving domain II and the major part of domain III (*21*) loses its ability to renature and restore its tertiary structure. According to the crystallographic data, the seventh α-helical region (domain 1) has a large area of contacts with domains II and III which stabilizes their tertiary structure (*33*). On the other hand, a Cry3A fragment (49 kDa) that has lost 57 amino acids from the C-end retains full insecticidal activity and exhibits specific binding to midgut membranes (*35*). Thus, it is very likely that the fragment holds its tertiary structure and the C-terminal part of β-sheet domain III is not essential for maintaining the native conformation of Cry3A δ-endotoxin. It should be mentioned that this is not correct for the Cry1A toxin. It was shown for mutants of the Cry1A toxin that removal of one or several amino acids from the C-end of the protein results in the formation of nontoxic products or polypeptides highly sensitive to proteolytic degradation (*1*, *43*). So we can conclude that removal of the N-terminal α-helical domain is the main reason for the loss of unique tertiary structure of the 37 kDa fragment. The nucleation core determining protein folding does not involve its three initial α-helices of the N-terminal domain but can include the remaining α-helices. Recently, a detailed description of transition states on the level of individual interactions has been provided by an extensive mutational and thermodynamic approach for barnase (*44*, *45*) and for chymotrypsin inhibitor 2 (*46*, *47*). Taken together, these data suggest that peripheral parts of the proteins are loosened up in the transition state whereas the centers of hydrophobic cores and some elements of secondary structure remain relatively intact. Our data are consistent with this result.

REFERENCES

1. Hofte, H., and Whiteley, H. R. (1989) *Microbiol. Rev. 53*, 242−255.
2. Feitelson, J. S., Payne, J., and Kim, L. (1992) *Bio/Technology 10*, 271−275.
3. Gill, S. S., Cowles, E. A., and Pietrantonio, P. V. (1992) *Annu. Rev. Entomol. 37*, 615−636.
4. Hofte, H., Seurink, J., van Houtven, A., and Vaeck, M. (1987) *Nucleic Acids Res. 15*, 7183−7186.
5. Carroll, J., Li, J., and Ellar, D. J. (1989) *Biochem. J. 261*, 99−105.
6. Knowles, B. H., and Ellar, D. J. (1987) *Biochim. Biophys. Acta 924*, 509−518.
7. Knowles, B. H. (1994) *Adv. Insect Physiol. 24*, 275−308.
8. Schwartz, J.-L., Juteau, M., Groshulski, P., Cygler, M., Prefontaine, G., Brousseau, R., and Masson, L. (1997) *FEBS Lett. 410*, 397−402.
9. Freire, E., and Biltonen, R. L. (1978) *Biopolymers 17*, 463−479.
10. Privalov, P. L. (1982) *Adv. Protein Chem. 35*, 1−104.
11. Privalov, P. L., and Potekhin, S. A. (1986) *Methods Enzymol. 131*, 1−51.
12. Kidokoro, S.-J., and Wada, A. (1987) *Biopolymers 26*, 213−229.
13. Freire, E., van Osdol, W. W., Mayorga, O. L., and Sanchez-Ruiz, J. M. (1990) *Annu. Rev. Biophys. Chem. 19*, 159−188.
14. Lepock, J. R., Ritchie, K. P., Kolios, M. C., Robahl, A. M., Heinz, K. A., and Kruuv, J. (1992) *Biochemistry 31*, 12706−12712.
15. Sanchez-Ruiz, J. M. (1992) *Biophys. J. 61*, 921−935.
16. Milardi, D., La Rosa, C., and Grasso, D. (1994) *Biophys. Chem. 52*, 183−189.
17. Loseva, O. I., Kirkitadze, M. D., Dobritsa, A. P., and Potekhin, S. A. (1996) *Bioorg. Khim. 22*, 785−790.
18. Chestukhina, G. G., Zalunin, I. A., Kostina, L. I., Kotova, T. S., Katrukha, S. P., and Stepanov, V. M. (1980) *Biochem. J. 187*, 457−465.
19. Mahillon, J., and Delcour, J. (1984) *J. Microbiol. Methods 3*, 69−76.
20. Thomas, W. E., and Ellar, D. J. (1983) *J. Cell Sci. 60*, 181−197.
21. Ort, P., Zalunin, I. A., Gasparov, V. S., Chestukhina, G. G., and Stepanov, V. M. (1995) *J. Protein Chem. 14*, 241−249.
22. Laemmli, U. K. (1970) *Nature 227*, 680−685.
23. Lowry, O. H., Rosenbrough, N. J., Farr, A. L., and Randall, R. J. (1951) *J. Biol. Chem. 193*, 265−275.
24. Vogl, T., Jatzke, C., Hinz, H.-J., Benz, J., and Huber, R. (1997) *Biochemistry 36*, 1557−1668.
25. Potekhin, S. A., and Kovrigin, E. L. (1998) *Biofizika 43*, 223−232.

26. Potekhin, S. A., and Kovrigin, E. L. (1998) *Biophys. Chem. 73*, 241−248.
27. Conejro-Lara, F., Sanchez-Ruiz, J. M., Mateo, P. L., Burgos, F. J., Vandrell, J., and Aviles, F. X. (1991) *Eur. J. Biochem. 200*, 663−670.
28. Sanchez-Ruiz, J. M., Lopez-Lacomba, J. L., Cortijo, M., and Mateo, P. L. (1988) *Biochemistry 27*, 1648−1652.
29. Privalov, P. L. (1979) *Adv. Protein Chem. 33*, 167−241.
30. Segawa, S., and Sugihara, M. (1984) *Biopolymers 23*, 2473−2488.
31. Chen, B., Baase, W., and Shellman, J. A. (1989) *Biochemistry 28*, 691−699.
32. Chen, B., and King, J. (1991) *Biochemistry 30*, 6260−6269.
33. Li, J., Carrol, J., and Ellar, D. J. (1991) *Nature 353*, 815−821.
34. Grochulski, P., Masson, L., Borisova, S., Pusztai-Carey, M., Schwartz, J.-L., Brousseau, R., and Cygler, M. (1995) *J. Mol. Biol. 254*, 447−464.
35. Carroll, J., Convents, D., Van Damme, J., Boets, A., Van Rie, J., and Ellar, D. J. (1997) *J. Invertebr. Pathol. 70*, 41−49.
36. McRee, D. E., Redford, S. M., Getzoff, E. D., Lepock, J. R., Hallewell, R. A., and Tainer, J. A. (1990) *J. Biol. Chem. 265*, 14234−14241.
37. Galisteo, M. L., Mateo, P. L., and Sanchez-Ruiz, J. M. (1991) *Biochemistry 30*, 2061−2066.
38. Schindler, T., and Schmid, F. X. (1996) *Biochemistry 35*, 16833−16842.
39. Tan, Y.-J., Oliveberg, M., and Fersht, A. R. (1996) *J. Mol. Biol. 264*, 377−389.
40. Oliveberg, M., and Fersht, A. R. (1996) *Biochemistry 35*, 2738−2749.
41. Jackson, S. E., and Fersht, A. R. (1991) *Biochemistry 30*, 10428−10435.
42. Shakhnovich, E. I., and Finkelstein, A. V. (1989) *Biopolymers 28*, 1667−1680.
43. Wabiko, H., and Yasuda, E. (1995) *Microbiology 141*, 629−639.
44. Matouschek, A., Kellis, J. T., Serrano, L., and Fersht, A. R. (1989) *Nature 342*, 122−126.
45. Serrano, L., Matouschek, A., and Fersht, A. R. (1992) *J. Mol. Biol. 224*, 805−818.
46. Otzen, D. E., Itzhaki, L. S., elMasry, N. F., Jackson, S. E., and Fersht, A. R. (1994) *Proc. Natl. Acad. Sci. U.S.A. 91*, 10422−10425.
47. Itzhaki, L. S., Daniel, E. O., and Fersht, A. R. (1995) *J. Mol. Biol. 254*, 260−288.

BI982789K